Mode matching for second-harmonic generation in photonic crystal waveguides

A. R. Cowan and Jeff F. Young
Department of Physics and Astronomy, University of British Columbia, Vancouver, British Columbia, Canada V6T 1Z4
(Received 5 September 2001; published 7 February 2002)

The influence of localized photonic eigenstates on the second-harmonic generation efficiency in planar photonic crystal waveguides is studied with a simple, yet realistic model. We show that $\geqslant 10^6$ enhancements in the *external* conversion efficiency in specular reflection can be achieved due to a combination of ''generalized phase-matching'' and strong local fields in these periodically textured, nonlinear dielectric structures. The second-harmonic response involving the resonant modes of these membranelike photonic crystals is essentially a resonant cavity effect, and hence is strongly influenced by the modal quality factor.

DOI: 10.1103/PhysRevB.65.085106 PACS number(s): 42.70.Qs, 42.65.Ky

I. INTRODUCTION

After several years of development work, photonic crystals (PC's: high-refractive-index dielectrics textured periodically in three or two dimensions) with optical band gaps in the near infrared are now becoming available.[1] Work on these artificial materials has been driven by the predictions of several phenomena that should be accessible given hosts in which the total density of photon modes is drastically altered from that characteristic of bulk dielectrics.[2–4] After the existence of full gaps was experimentally verified at microwave frequencies,[5] for which relevant crystals can be made quite easily, much effort focused on structures with submicron lattice constants needed for the gap to be in frequency ranges relevant to optical communications and convenient light sources. Based on designs which predict a complete gap at around 1.55 μm, three-dimensional (3D) crystals of silicon were recently realized that exhibit reflectivity spectra in qualitative agreement with theory.[1]

While many practical applications are likely to be found for the unique *linear* optical properties of both bulk and defect states in PC's, it is their *nonlinear* optical properties that are particularly exciting from the perspective of light-matter interactions. Interesting photon-atom bound states that possess intriguing coherence characteristics were predicted to exist when an atomic transition lies in the vicinity of a model photonic band edge, where the excluded photonic states are assumed to bunch.[6–9] However, further work suggested that these phenomena are sensitive to the detailed form of the photon density of states near the band edge.[10] Therefore, it appears that rigorous rather than phenomenological treatment of the actual photonic dispersion is important. The detailed structure of the photonic states was successfully included in studies of nonlinear propagation through both 1D (Refs. 11–15) and 2D (Refs. 16–19) periodic material, mediated by a nonzero $\chi^{(2)}$ in the underlying bulk. A thorough review of the 1D work was presented in Ref. 15. In comparison to the nonlinear conversion that occurs when propagating in homogeneous bulk materials, a regular periodic modulation of either or both of $\chi^{(1)}$ and $\chi^{(2)}$ offers significant flexibility in achieving phase matching, through the ''generalized phase matching condition'' $\vec{\beta}(2\omega)=2\vec{\beta}(\omega)+\vec{G}_i$, where $\vec{G}_i$ is one of the reciprocal-lattice vectors that describes the periodic modulation, and $\vec{\beta}$ is the propagation wave vector. This is relevant for keeping the fundamental and second-harmonic fields properly phased, as they propagate through the nonlinear medium. When phase matching is achieved, the effective nonlinear conversion per unit length of propagation can be enhanced in periodic materials by purposely coupling to modes with low group velocity, at energies for which there is an enhanced density of states. Finally, the best overall conversion is achieved when there is good spatial overlap between the fundamental and second harmonic modes.

Although they can not possess true optical band gaps, 2D photonic crystal structures etched into semiconductor waveguides are also of substantial interest, due in part to the relative ease of working at submicrometer length scales in two dimensions, and because they are directly compatible with the extensive waveguide-based optoelectronics industry. Figure 1 shows the calculated 2D band structure of the photonic eigenstates along the Γ-X direction of a freestanding, 130-nm-thick GaAs waveguide. It has been textured with a square array of air holes, 202 nm in radius, with a spacing of $\Lambda=800$ nm, that extend through the entire guide. The grating wave vector is $\beta_g=2\pi/\Lambda$. Solid (s-polarized) and dashed (p-polarized) lines represent bound (outside or below the light cone) and resonant (inside or above the light cone) modes that are substantially localized to the textured waveguide. For clarity we have only plotted the bands relevant to the nonlinear conversion process considered below. The shaded area inside the light cone contains a continuum of radiation modes that have comparable field strengths inside and outside the slab waveguide. All modes within the light cone can be conveniently excited by radiation incident on the waveguide from the upper half space (UHS). The dispersion of resonant electromagnetic modes attached to planar photonic crystals (PPC's) have been measured using a number of techniques,[20–23] and we recently demonstrated excellent quantitative agreement with theory.[23] True bound modes outside the light cone can only be excited using a prism, a grating, or butt coupling to provide the additional in-plane momentum.

The fundamental nature of nonlinear conversion involving true bound modes in this geometry will be similar to that already worked out for bulk 2D photonic crystals, but the actual conversion efficiencies would have to be evaluated using the appropriate eigenstates. Phase matching and propagation would be strictly limited to the plane of the textured

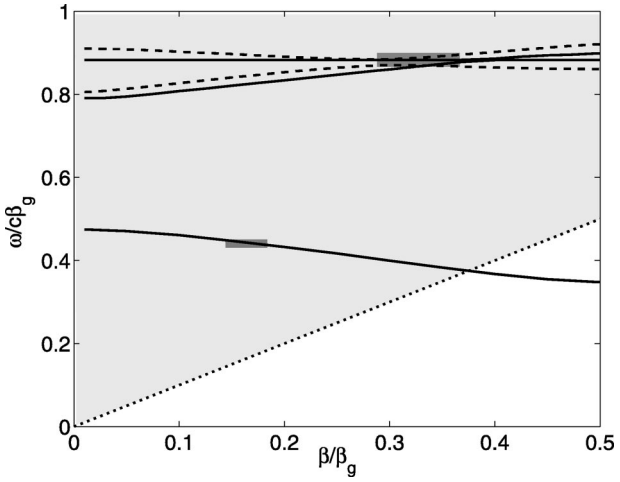

FIG. 1. Linear photonic band structure along the *X* direction of the first Brillouin zone for the free-standing photonic crystal waveguide described in the text. For clarity we only show the bands involved in our SHG calculation. Solid curves denote *s*-polarized modes, and dotted curves *p*-polarized modes. The shading represents the continuum of radiation modes. The two shaded boxes show the areas of phase space involved in the second-harmonic generation calculation.

slab. In contrast, the resonant modes, remnants of the bound modes that exist within the vacuum light cone, offer a distinctly different type of nonlinear conversion involving periodic media. When both fundamental and second-harmonic fields lie within the vacuum light cone, the problem is not one of conversion versus distance in the direction of propagation, but rather one of an engineered enhancement of what is effectively surface second harmonic generation. As we show below, uniform illumination from the top half-space can resonantly excite large local fields in the vicinity of the textured membrane, which can in turn be efficiently coupled back out in the form of an outward propagating plane wave in vacuum. It turns out that the overall external efficiency of this reflective harmonic conversion process, which our model calculates in a completely self-consistent manner, can be understood as a sort of virtual phase matching within the nonlinear photonic crystal cavity, that has nothing directly to do with in plane propagation effects.

In Sec. II we describe the process of second-harmonic generation of plane waves incident on this thin periodic structure, and introduce our theoretical approach to self-consistently solving for the second-harmonic field. In Sec. III a sample calculation is presented that quantitatively illustrates the effect of the periodicity. Section IV elaborates on how the conversion efficiency depends on the *Q* value of the relevant photonic modes. Conclusions are presented in Sec. V.

II. THEORY

If the free-standing textured waveguided described in Sec. I is irradiated from above with light at a certain frequency ω and some arbitrary in-plane momentum $\vec{\beta}_{inc}$, the light will more often than not merely be transmitted without generating any significant fields in the guiding region. The second-order polarization it excites in the waveguide, through a nonzero $\chi^{(2)}(-2\omega;\omega,\omega)$, would then be comparable to that which would be excited in an untextured version of the same waveguide. If the frequency 2ω and in-plane wave vector $2\vec{\beta}_{inc}$ of this nonlinear polarization do not coincide with one of the lines in Fig. 1, then the polarization will also couple out of the guide in much the same way it would in the absence of texture. The overall second-harmonic generation (SHG) conversion efficiency for this process in GaAs is small. If, on the other hand, either or both of the fields at $(\omega,\vec{\beta}_{inc})$ and $(2\omega,2\vec{\beta}_{inc})$ coincide with the localized mode dispersion, then the conversion efficiency can be significantly enhanced due to the excitation of strong local fields associated with resonant photonic modes of the textured waveguide. The textured membrane can be thought of as a 1D microcavity (the slab itself), with additional modification of the photonic density of states provided by the strong 2D texture. Modes of this cavity that lie within the vacuum light cone couple (*grating couple*) to plane waves that radiate in the surrounding half-spaces. This radiative coupling determines the lifetimes, or the *Q*'s of these cavity modes. Weakly coupled modes with high *Q*'s will accumulate significant local field intensities when excited from the vacuum, much like conventional planar Fabry-Perot cavities excited on resonance. The advantage of this grating coupling geometry is that the total internal reflection that confines the dominant (evanescent) field components of the resonant eigenstates does not require the fabrication of multilayer Bragg reflectors above and below the cavity layer. This confining mechanism, characteristic of these waveguide-based photonic crystals, is responsible for extremely large enhancements in the conversion efficiency: as shown below, even with no attempt at optimization, the effect of texturing the waveguide can cause an enhancement of the reflected second harmonic by at least $\approx 10^6$.

In addition to enhancements of the magnitude of the radiated second harmonic, it is important to understand the polarization conversion rules. These conversions are sensitive to the symmetries and relative orientations of the photonic and electronic lattices. For example; in this paper we consider the nonlinear waveguide to be the semiconducting material GaAs, and the photonic crystal to be of square symmetry. The GaAs crystal is of cubic symmetry, and a member of the $\bar{4}3m$ point group. For arbitrary orientations of the two lattices, either *s*- or *p*-polarized incident radiation will in general produce an elliptically polarized second harmonic field. For specific orientations of the two lattices, further symmetry considerations dictate simplified polarization properties. When the [001] axis of the GaAs crystal is aligned with the *X* axis of the square symmetric photonic lattice, it is not possible to excite *p*-polarized second-harmonic modes along the Γ-*X* direction of the square Brillouin zone. Likewise, for the same orientation of the two lattices, no *s*-polarized second harmonics are generated along the Γ-*M* direction. Thus along these symmetry axes, the fundamental polarization will either be preserved or rotated by 90° in the second harmonic when the photonic and electronic crystal axes are aligned.

The calculation of the radiated second harmonic from arbitrary 2D textured PPC proceeds as follows. Taking the periodic polarization in the textured region as a driving term, Maxwell's equations, in the waveguide geometry, are solved using a Green's-function technique. When a plane wave with frequency $\tilde{\omega}=\omega/c$ and in-plane wave vector $\vec{\beta}_{inc}$ is incident from the upper half-space, the self-consistent solution for a single Fourier component of the field in the grating is given by

$$\vec{E}(\tilde{\omega},\vec{\beta}_i,z)=\vec{E}^{hom}(\tilde{\omega},\vec{\beta}_i,z)+\int dz'\vec{\vec{g}}(\vec{\beta}_i,\tilde{\omega},z,z') \times\sum_j \vec{\vec{\chi}}^{(1)}_{ij}(-\tilde{\omega},\tilde{\omega})\vec{E}(\tilde{\omega},\vec{\beta}_j,z'), \quad (1)$$

where $\vec{\beta}_i=\vec{\beta}_{inc}-\vec{G}_i$ is the in-plane wave vector of the Fourier component, and $\vec{G}_i$ are the reciprocal-lattice vectors. The periodic susceptibility has been expanded as a Fourier series with coefficients $\vec{\vec{\chi}}_{ij}$ (i.e., $\vec{\vec{\chi}}_{ij}=\int d\vec{\rho}\,\vec{\vec{\chi}}(\vec{\rho})\exp[-i(\vec{G}_i-\vec{G}_j)\cdot\vec{\rho}]$). By approximating a finite number N of Fourier components for the in-plane field structure, and a textured region that is sufficiently thin so that the fields can be taken as constant over its extent, the infinite set of vector integral equations implied in Eq. (1) are reduced to a finite set of scalar algebraic equations of size $3N$. If required, thick gratings can be modeled by splitting the region into l thinner regions, each of which satisfy the constant field approximation. The simple matrix algebra required for the solution of the $3Nl$ set of equations, and the derivation of the Green's function $\vec{\vec{g}}(\vec{\beta}_i,\tilde{\omega},z,z')$, are described in detail (for $l=1$) in Ref. 24.

These Fourier field components are then used as the source fields in calculating the Fourier components of the second-order polarization in the textured region:

$$\vec{P}^{(nl)}(2\tilde{\omega},\vec{\beta}_n,z)=\sum_{m,l}\vec{\vec{\chi}}^{(2)}_{nm}(-2\tilde{\omega},\tilde{\omega},\tilde{\omega}):$$

$$\vec{E}(\tilde{\omega},\vec{\beta}_{inc}-(\vec{G}_m-\vec{G}_l),z)\vec{E}(\tilde{\omega},\vec{\beta}_{inc}-\vec{G}_l,z). \quad (2)$$

The in-plane wave vectors of $\vec{P}^{(2)}(\vec{\beta}_n)$ are given by $\vec{\beta}_n=2\vec{\beta}_{inc}-\vec{G}_n$. Using both this nonlinear polarization, as well as the linear polarization at $[(2\tilde{\omega},\vec{\beta}_n)]$ as driving terms, the Fourier components of the second-harmonic field in the grating can be self-consistently calculated using a similar Green's-function approach. Therefore, within the undepleted pump approximation, the second-harmonic Fourier components in the grating satisfy

$$\vec{E}(2\tilde{\omega},\vec{\beta}_n,z)=\int dz'\vec{\vec{g}}(\vec{\beta}_n,2\tilde{\omega},z,z') \times\left[\sum_m \vec{\vec{\chi}}^{(1)}_{nm}(-2\tilde{\omega},2\tilde{\omega})\vec{E}(2\tilde{\omega},\vec{\beta}_m,z') + \vec{P}^{(nl)}(2\tilde{\omega},\vec{\beta}_n,z')\right]. \quad (3)$$

Approximating N' Fourier component for the in-plane field structure, and l' thin textured and/or nonlinear regions over which the field is effectively constant, Eq. (3) is reduced to a system of $3N'l'$ algebraic equations and solved with an analogous matrix method as was used for Eq. (1).

The Fourier components of the total second-harmonic field in the textured regions are then transferred to the top surface of the structure by

$$\vec{E}_{UHS}(2\tilde{\omega},\vec{\beta}_n,z_t) =\sum_{i=1\ldots l'}\int_{z_o^i-t_g^i/2}^{z_o^i+t_g^i/2}dz'\vec{\vec{g}}_{UHS,i}(\vec{\beta}_n,2\tilde{\omega},z_t,z') \times\left[\sum_m \vec{\vec{\chi}}^{(1)}_{nm}\vec{E}(2\tilde{\omega},\vec{\beta}_m,z_o^i)+\vec{P}^{(nl)}(2\tilde{\omega},\vec{\beta}_n,z_o^i)\right], \quad (4)$$

where z_t denotes the surface of the structure, z_o^i and t_g^i, respectively, denote the center and thickness of textured region i, and $\vec{\vec{g}}_{UHS,i}$ is the Green's function which propagates the fields from inside region i to the surface; it was also derived in Ref. 24. The field $\vec{E}(2\tilde{\omega},\vec{\beta}_m,z_o^i)$ is the total field in the textured region and is self-consistently given by Eq. (3). Upon making approximations analogous to the ones above, Eq. (4) is solved using a similar matrix method.

III. SAMPLE CALCULATION

With the use of one simple example, we now illustrate the enhancement and polarization properties of SHG in photonic crystal waveguides. Consider the symmetric, free-standing, waveguide described above. While Fig. 1 shows the linear band structure, Fig. 2 shows the region of the band structure over which we calculate the second-harmonic fields. In Fig. 2, the solid curve is the low-frequency *s*-polarized mode from Fig. 1, while the dashed and dotted curves are the high-frequency *p*- and *s*-polarized modes *plotted at half their frequency and in-plane wave vector*, respectively.

As we consider incident radiation oriented along the X axis of the photonic crystal, the solid curve in Fig. 2 represents the photonic band with which the fundamental field can be resonant. Likewise, the dashed and dotted curves represent higher-lying photonic bands with which the second harmonic can be resonant when the fundamental has the frequency and in-plane wave vector given by the axes' values. If the fundamental falls on the solid curve there will be a resonant to nonresonant SHG conversion process, meaning that the fundamental is resonant with a photonic mode and the second harmonic is non-resonant. Likewise, if the fundamental's frequency and in-plane wave vector fall on a dashed or dotted curve in Fig. 2, then there will be a nonresonant to resonant SHG conversion process. The resonant to resonant SHG process (denoted by circles in Fig. 2) occurs when one of the dashed or dotted curves crosses the solid curve. This resonant to resonant condition results in a fully mode-matched nonlinear conversion process, effectively allowed in this periodic geometry by Bloch's theorem, or a ''quasi-phase-matching'' condition. Note, for simplicity, that the index of refraction of GaAs was taken to be 3.5 throughout the

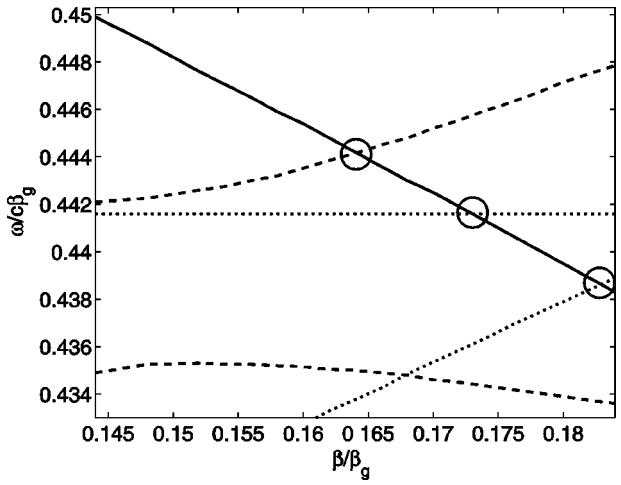

FIG. 2. An enlarged and overlapped depiction of the two rectangular regions in Fig. 1. The solid curve is the low frequency *s*-polarized band in Fig. 1. The dashed and dotted curves are the high-frequency *p*- and *s*-polarized bands, respectively, plotted at half their frequency and in-plane momentum. Circles denote points where fully mode-matched nonlinear conversion can occur.

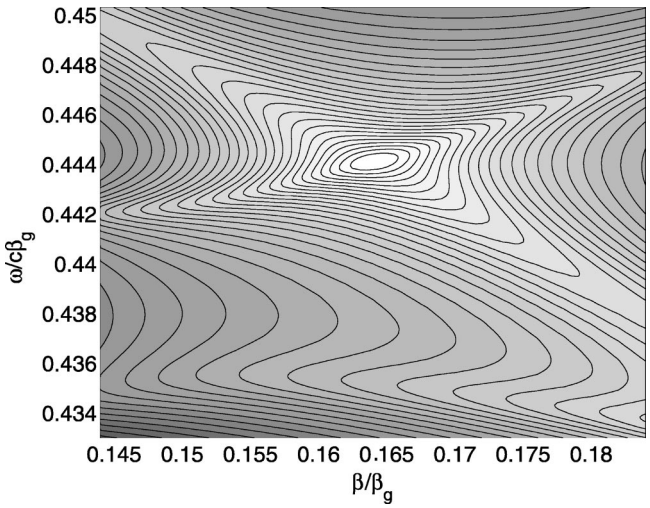

FIG. 3. Radiated second harmonic from the free-standing photonic crystal waveguide described in the text. The figure plots $\log[|\vec{E}_{UHS}(2\tilde{\omega},\vec{\beta}_{spec},z_t)|^2]$ as a function of the fundamental frequency and in-plane wave vector for the *s*-*p* scattering process. Contours show an enhancement in the radiated second harmonic when the fundamental frequency and in-plane wave vector intersect one of the bands in Fig. 2. Each contour corresponds to 3.92 dB.

calculation. If the actual refractive indices at both ω and 2ω were used, the location of the enhanced peaks would shift slightly, but the physical processes leading to these enhancements would be unchanged.

Figure 3 plots the intensity of the second-harmonic field radiated into the UHS when the incident fundamental field is *s* polarized, and the output second harmonic field is *p* polarized (*s*-*p* scattering). The calculation covers the same area of the first Brillouin zone shown in Fig. 2. Figure 3 is a plot of $\log[|\vec{E}_{UHS}(2\tilde{\omega},\vec{\beta}_{spec},z_t)|^2]$ as a function of the fundamental frequency $\tilde{\omega}$ and fundamental in-plane wave vector β_x ($\beta_y=0$ as we have taken the incident field to be along the photonic crystal's *X* axis). The subscript ''spec'' denotes the component of the field which is phase matched to radiate into the UHS in the specular direction. The incident field intensity is taken to be 1 stv/cm, which corresponds to an intensity of 475 W/cm^2. For this calculation the 130-nm grating was split into two 65-nm-thick gratings [$l'=2$ in Eq. (4)]. These two layers produced well-converged results; converged in the sense that calculations with three layers gave the same results up to a fraction of a percent. This *s*-*p* scattering is allowed only because we have taken the [001] axis of the GaAs crystal to be rotated by 20° with respect to the photonic crystal.

The contours in Fig. 3 illustrate the enhancement in the magnitude of the radiated second harmonic when either the fundamental or second-harmonic fields are resonant with photonic modes. Note the ridges that follow the solid and dashed curves of Fig. 2. Away from these resonant conversions we find the magnitude of the radiated second harmonic to be nominally the same as an untextured waveguide. The greatest enhancement in the second harmonic occurs at the resonant to resonant condition.

At the resonant to resonant condition in Fig. 3, ($\tilde{\omega}/\beta_g=0.444, \beta/\beta_g=0.164$), the peak intensity is 1.5×10^{-9}(stv/cm)^2,[25] or 7.1×10^{-7} W/cm^2, 3.83×10^6 times greater than the maximum intensity radiated from an untextured version of the same waveguide. For the resonant to nonresonant and nonresonant to resonant conversion processes, we find enhancements on the order of 10^2–10^4 over the untextured waveguide value. These enhancements are particular to this structure and these specific photonic modes, and have not been optimized in any way. With a detailed study of a structure's band structure and the modal lifetimes, these enhancements could undoubtedly be optimized.

Figures 4 and 5 show 3D plots of the intensity of the radiated second harmonic for the *s*-*p* and *s*-*s* scattering processes, respectively. The vertical axis is the intensity of the field on a linear scale in units of (stv/cm)^2 for an incident field intensity of 1 (stv/cm)^2. In Fig. 4 (*s*-*p* scattering) the large enhancement of the second harmonic at the mode-matched condition, as shown in the contour plot of Fig. 3, is obvious. In Fig. 5, we again find an enhancement when each of the relevant fields is separately resonant with a photonic mode. Note that for the *s*-*s* scattering process the ridges now follow the *s*-polarized second-harmonic modes instead of the *p*-polarized modes, as was the case in Figs. 3 and 4. This is due to the photonic modes having a well-defined *s* or *p* polarization. For this scattering process the nonresonant to resonant conversion is still enhanced by approximately 10^3, but the resonant to nonresonant enhancement is on the order of 10^5. The dominate feature in the *s*-*s* spectrum therefore follows the incoming photonic mode dispersion. In this case the completely mode-matched condition does not provide much more enhancement than the resonant to nonresonant process.

In light of these results, when coupling in and out of planar photonic crystals via the resonant modes that lie within the vacuum light cone, it is clear that the second-

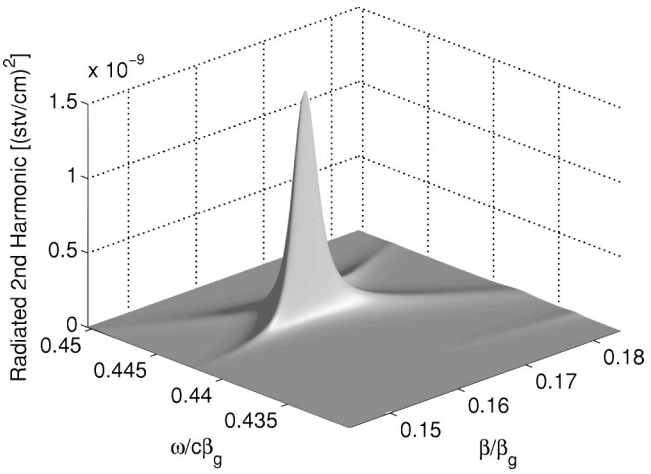

FIG. 4. Plot of the *s*-*p* radiated second harmonic. The intensity of the second harmonic is expressed in $(\mathrm{stv/cm})^2$, the incident field is assumed to have an intensity of 1 $(\mathrm{stv/cm})^2$, and the value for $\chi^{(2)}$ is 238 pm/V.

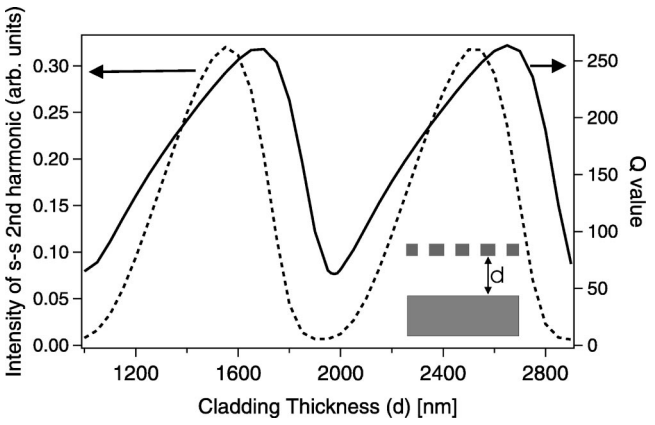

FIG. 6. The dependence of the radiated second harmonic on the *Q* of the incoming photonic mode. The solid curve is the *Q* value of the fundamental *s*-polarized mode (right axis), and the dashed curve is the peak intensity of the *s*-*s* radiated second harmonic (left axis). The inset depicts a schematic cross section of the PPC, illustrating which layer thickness is being varied.

harmonic conversion process is essentially a resonant cavity effect,[28] as opposed to the propagation effect previously considered in the literature.[16,12,13,15,18] However, because the resonant coupling to the cavity is mediated by scattering from the dielectric texture, our analysis shows that the internal conversion process is optimized by using the same generalized phase-matching condition that would apply in the propagating geometry. The absolute external conversion efficiency under phase-matched conditions depends on the internal conversion efficiency between the incoming and outgoing modes, on the coupling efficiency of the outgoing mode to the upper half-space, and on the local field enhancement associated with the incoming resonance (the *Q* of the mode). In a completely self-consistent formalism it is difficult to isolate these separate effects completely. However, the incoming coupling is identical along the *s*-polarized band in both Figs. 4 and 5. It is therefore clear that there can be substantial differences in the overall conversion efficiency, due to a combination of the internal mode conversion efficiency, and the outgoing mode's coupling to the top half-space. However, one might expect that the most effective way to engineer the conversion efficiency would be by controlling the effective *Q* value for the incoming mode, due to the nonlinear dependence of the conversion process on the local field enhancement at the fundamental frequency. In Sec. IV we use a slightly modified PC membrane structure to illustrate how the enhancement factor depends on the *Q* of the incoming photonic mode.

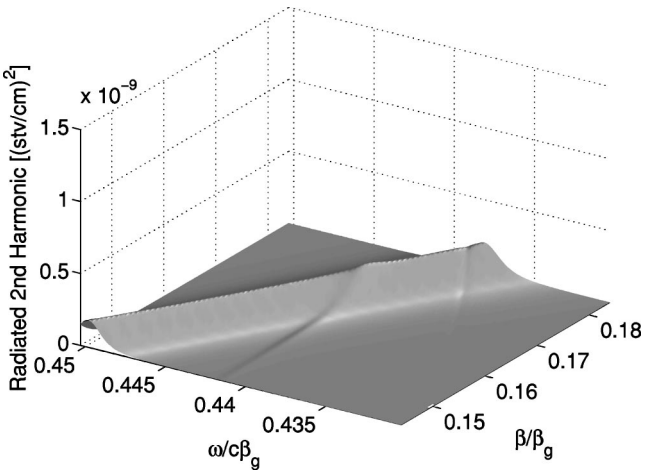

FIG. 5. Plot of the *s*-*s* radiated 2nd harmonic. The intensity of the second harmonic is expressed in $(\mathrm{stv/cm})^2$, the incident field is assumed to have an intensity of 1 $(\mathrm{stv/cm})^2$, and the value for $\chi^{(2)}$ is 238 pm/V.

IV. EFFECT OF THE CAVITY *Q* OF THE INCOMING MODE

We have previously shown that the Q factor for a given photonic band can vary significantly due to effects of symmetry, and due to mode coupling both within, and perpendicular to, the textured plane.[27,23,24] There are therefore several ways to engineer a textured slab so as to achieve both generalized phase matching and high-*Q* incoming resonances. Here we do not attempt this optimization process; instead we use a pedagogical tool to try and isolate the effect of the incoming cavity *Q*.

In an attempt to keep the internal conversion efficiency and phase-matching conditions fixed, while substantially varying the *Q* of the incoming resonance, we repeat our model calculations for the same 130-nm-thick textured slab, but now include a remote GaAs substrate, separated from the textured slab by an air gap with variable thickness *d* (see the inset to Fig. 6). This approach is based on previous work (Ref. 24), where we reported that the linewidth of resonant coupling in 2D textured planar waveguides can be controlled over a wide range by varying the location of the grating within the slab waveguide structure, while leaving the resonant frequency almost unchanged. The linear band structure of this modified structure is effectively the same as shown in Fig. 1, so long as the vacuum layer thickness is greater than

the evanescent decay length of the modes attached to the slab. However the Q of the incoming s-polarized resonance changes substantially as the thickness of the vacuum cavity is varied, as shown by the solid curve in Fig. 6.

The dashed curve in Fig. 6 shows the intensity of the upward-propagating component of the second-harmonic field generated by the fundamental mode excited in this geometry. The second-harmonic field is for the s-s scattering process, and the in-plane wavevector is held constant at $\vec{\beta}/\beta_g = 0.164\hat{x}$ as the cladding thickness was adjusted. The strength of the second harmonic clearly correlates strongly with the Q of the incoming resonance. The slight phase shift is due to the fact that some of the other factors involved in the self-consistent calculation are also influenced by the vacuum cavity, but to a much smaller extent. In optimizing the design of such a structure, it is therefore advisable to seek a high-Q incoming resonance at the generalized phase matched condition.

It should be noted that the calculations presented in this paper assume plane waves incident on PPC's that are infinite in lateral extent. In actual experiments, there would be a broadening of the modes and a decrease in the enhancement factors due to the finite-size of the incident optical beam and due to the size of the crystal. There is no universal factor that describes this finite-size effect as it depends on both the dispersion and Q of the modes concerned. Nevertheless, it is likely that samples on the order of 1 mm in extent would be required to observe the largest enhancements reported above.

V. CONCLUSIONS

In summary, we have studied the efficiency of second harmonic reflection of plane waves incident on 2D textured semiconductor membranes. The influence of leaky photonic eigenstates attached to the porous membranes is evaluated using a Green's-function technique that self-consistently includes both linear and nonlinear polarizations in one heuristic calculation. The combined effects of quasi-phase-matching and strongly localized photonic modes allow for large enhancements in the nonlinear conversion efficiency. We explicitly demonstrate the strong dependence of the second-harmonic conversion efficiency on the Q factor of the incoming resonance, illustrating that this is essentially a nonlinear cavity effect. The basic formalism can be easily extended to higher-order nonlinear processes, and to include the truly bound (infinitely long lived) modes outside of the light cone.

ACKNOWLEDGMENTS

We wish to thank NSERC and Galian Photonics Inc. for their financial support of this work.

[1] A. Blanco, E. Chomski, S. Gradtchak, M. Ibisate, S. John, S. W. Leonard, C. Lopez, F. Meseguer, H. Miguez, J. P. Mondia, G. A. Ozin, O. Toader, and Henry M. van Driel, Nature (London) **405**, 437 (2000).
[2] S. John, Phys. Rev. Lett. **58**, 2486 (1987).
[3] E. Yablonovitch, Phys. Rev. Lett. **58**, 2059 (1987).
[4] J. D. Joannopoulos, Pierre R. Villeneuve, and Shanhui Fan, Nature (London) **386**, 143 (1997).
[5] E. Yablonovitch, T. J. Gmitter, and K. M. Leung, Phys. Rev. Lett. **67**, 2295 (1991).
[6] S. John and J. Wang, Phys. Rev. B **43**, 12 772 (1991).
[7] T. Quang, M. Woldeyohannes, S. John, and G. S. Agarwal, Phys. Rev. Lett. **79**, 5238 (1997).
[8] H. G. Winful and V. Perlin, Phys. Rev. Lett. **84**, 3586 (2000).
[9] S. John and T. Quang, Phys. Rev. Lett. **76**, 2484 (1996).
[10] Zhi-Yuan Li, Lan-Lan Lin, and Zhao-Qing Zhang, Phys. Rev. Lett. **84**, 4341 (2000).
[11] J. Trull, R. Vilaseca, Jordi Martorell, and R. Corbalan, Opt. Lett. **20**, 1746 (1995).
[12] C. De Angelis, F. Gringoli, M. Midrio, D. Modotto, J. S. Aitchison, and G. F. Nalesso, J. Opt. Soc. Am. B **18**, 348 (2001).
[13] M. J. Steel and C. Martijn de Sterke, Appl. Opt., **35**, 3211 (1996).
[14] M. Centini, C. Sibilia, M. Scalora, G. D'Aguanno, M. Bertolotti, M. J. Bloemer, C. M. Bowden, and I. Nefedov, Phys. Rev. E **60**, 4891 (1999).
[15] M. Scalora, M. J. Bloemer, A. S. Manka, J. P. Dowling, C. M. Bowden, R. Viswanathan, and J. W. Haus, Phys. Rev. A **56**, 3166 (1997).
[16] K. Sakoda and K. Ohtaka, Phys. Rev. B **54**, 5742 (1996).
[17] V. Berger, Phys. Rev. Lett. **81**, 4136 (1998).
[18] Jordi Martorell, R. Vilaseca, and R. Corbalan, Appl. Phys. Lett. **70**, 702 (1997).
[19] Joshua N. Winn, Shanhui Fan, John D. Joannopoulos, and Erich P. Ippen, Phys. Rev. B **59**, 1551 (1999).
[20] V. N. Astratov, D. M. Whittaker, I. S. Culshaw, R. M. Stevenson, M. S. Skolnick, T. F. Krauss, and R. M. De La Rue, Phys. Rev. B **60**, R16 255 (1999).
[21] D. Labilloy, H. Benisty, C. Weisbuch, C. J. M. Smith, T. F. Krauss, R. Houdre, and U. Oesterle, Phys. Rev. B **59**, 1649 (1999).
[22] M. Boroditsky, R. Vrijen, T. F. Krauss, R. Coccioli, R. Bhat, and E. Yablonovitch, J. Lightwave Technol. **17**, 2096 (1999).
[23] V. Pacradouni, W. J. Mandeville, A. R. Cowan, P. Paddon, Jeff F. Young, and S.R. Johnson, Phys. Rev. B **62**, 4204 (2000).
[24] A. R. Cowan, P. Paddon, V. Pacradouni, and Jeff F. Young, J. Opt. Soc. Am. A **18**, 1160 (2001).
[25] We assume the value of $\chi^{(2)}$ for GaAs to be 238 pm/V (Ref. 26). Since the incident field is assumed to have an amplitude of 1 stv/cm or 475.6 W/cm^2, and the corresponding intensity of the second harmonic is 7.08×10^{-7} W/cm^2, we conclude that the approximation of an undepleted pump is valid.
[26] *Nonlinear Optics in Semiconductor II*, edited by E. Garmire and A. Kost, Semiconductors and Semimetals Vol. 59 (Academic Press, Toronto, 1999), p 33.
[27] P. Paddon and Jeff F. Young, Phys. Rev. B **61**, 2090 (2000).
[28] This resonant cavity effect was discussed in the context of weak 1D gratings on waveguides by E. Popov and M. Neviere, J. Opt. Soc. Am. B **11**, 1555 (1994).